On the motion of inertial particles by sound waves

Jay Cleckler, Said Elghobashi, and Feng Liu
Department of Mechanical and Aerospace Engineering, University of California, Irvine, California 92697, USA

(Received 20 June 2011; accepted 27 February 2012; published online 23 March 2012)

This paper describes the numerical simulation of the motion of a heavy spherical particle in an acoustic wave using the equation of motion for a point particle. Our results agree well with the recent experimental data of Gonzàlez, Hoffmann, and Gallego ["Precise measurements of particle entrainment in a standing-wave acoustic field between 20 and 3500 Hz," J. Aerosol Sci. **31**, 1461–1468 (2000)]. Our simulations cover a range of particle relaxation number, $\tau^* = \omega\tau$, where τ is the particle relaxation time and ω is the angular acoustic frequency from 0.06 to 10, particle to fluid density ratios, ρ_p/ρ_f, from 2500 to 2, and moderate acoustic velocity amplitudes. The results show that the Stokes force controls particle motion for $\tau^* < 1$ and $\rho_p/\rho_f > 25$. Within this regime it is appropriate to consider the Basset, pressure gradient, and virtual mass forces as "higher order" corrections to the Stokes force. The magnitude of the Basset force exceeds that of the Stokes force for $\rho_p/\rho_f \geq 25$ and $\tau^* \geq 4$. All the forces in the particle equation of motion should be accounted for when simulating particle motion in an acoustic wave for $\rho_p/\rho_f < 25$. © *2012 American Institute of Physics*. [http://dx.doi.org/10.1063/1.3696243]

I. INTRODUCTION

The prevailing motion of a small inertial particle in a sound wave is periodic at the frequency of the sound wave, and with a velocity amplitude approaching that of the fluid velocity.

The effects of sound waves on particle dispersion are of interest in several applications. Inertial particles extract momentum from an acoustic wave and are thus responsible for the attenuation of sound over long propagation distances in the atmosphere or short distances in dusty flows. The oscillations of particles in a sound wave have been used as a technique for particle size measurement. Particle oscillation is also the basis of sonically induced particle agglomeration, a complex physical effect that has been used to collect small particles from gaseous flows.

We consider only small spherical aerosol particles whose Reynolds number, Re_p, is $\ll 1$, and whose diameters are much smaller than the acoustic wavelengths. Under these conditions, the periodic motion of particles has been approximated in many studies by accounting only for the Stokes drag force. However, the range of validity of this assumption has not been established. The purpose of this paper is to investigate the conditions under which a linearized Stokes drag model is appropriate. We perform numerical simulations of the Lagrangian motion of a "point particle" subjected to prescribed unsteady forces in an acoustic wave.

II. PREVIOUS RESEARCH

Basset,[1] Boussinesq,[2] and Oseen[17] studied the unsteady motion of a sphere in a stagnant, incompressible, and viscous fluid. Maxey and Riley[12] derived an equation for a sphere moving in a fluid under the two conditions: $Re_p \equiv \frac{|\mathbf{u}\text{-}\mathbf{v}|d_p}{\nu} \ll 1$ and $\frac{d_p^2}{\nu}\frac{U_0}{L} < 1$, where $|\mathbf{u}\text{-}\mathbf{v}|$ is the magnitude of the fluid velocity relative to the particle velocity, d_p: particle diameter, ν: fluid kinematic viscosity, U_0: velocity scale, and L: characteristic length over which the fluid velocity changes appreciably. The second condition states that the momentum diffusion time scale must be smaller than the convection time scale in the vicinity of the particle. This condition would be invalid for sound waves with

sufficiently high frequency and thus our study considers only acoustic frequencies for which the second condition is true. The particle velocity equation of Maxey and Riley[12] is

$$m_p \frac{dv_i}{dt} = 3\pi d_p \mu (u_i - v_i) + \frac{3}{2}\pi d_p^2 \mu \int_0^t \frac{\frac{d}{ds}(u_i - v_i)}{\sqrt{\pi \nu (t-s)}} ds + m_f \frac{Du_i}{Dt} + \frac{1}{2} m_f \frac{d}{dt}(u_i - v_i) - \frac{\pi d_p^3}{6}(\rho_p - \rho_f) g, \quad (1)$$

where m_p: particle mass, m_f: fluid mass displaced by the particle, v_i: particle velocity in the ith direction, u_i: fluid velocity in the ith direction, μ: fluid dynamic viscosity, ρ_f: fluid density, ρ_p: particle density, and g: acceleration of gravity.

The fluid velocity and its derivatives in Eq. (1) are evaluated at the location of the particle and therefore Eq. (1) is nonlinear for spatially varying fluid velocity. Du_i/Dt is the total derivative following a fluid particle. The first term on the RHS of Eq. (1) is the Stokes drag force. The second term, due to Basset, is the unsteady viscous drag. The third term accounts for the effects of pressure gradient on point particles. The fourth term accounts for the force required to displace fluid as the particle moves and is known as the virtual mass force. The last term accounts for buoyancy effects in a gravity field. Faxen forces[5] are neglected as they scale with the fourth power of particle diameter.

The development of a simplified equation for particle motion in a sound wave has been considered by numerous authors. The early history of this development is summarized by Mednikov.[13] The model commonly used is due to Brandt, Freund, and Hiedemann,[3] who derived a simple equation for the particle oscillation velocity by neglecting all but a linearized Stokes force,

$$\frac{v_p}{U_0} = \cos(\phi_0) \sin(kx \pm \omega t \pm \phi_0), \quad (2)$$

where v_p: particle velocity, U_0: acoustic velocity amplitude, ω: angular frequency, k: acoustic wave number, ϕ_0: $\arctan(\omega\tau)$, and τ: particle relaxation time.

To derive Eq. (2) from Eq. (1), the Stokes drag is linearized by prescribing the fluid velocity at the particle's initial location and neglecting all other forces. The model of Brandt, Freund, and Hiedemann (hereinafter referred to as the BFH model) predicts oscillatory particle motion at the acoustic driving frequency. The predicted velocity amplitude of particle motion is smaller than the fluid velocity amplitude. Additionally, the phase of the particle oscillations is delayed relative to that of the fluid.

Gucker and Doyle[7] performed controlled experiments on silicate particles and found their oscillations to be comparable to the predictions of Brandt *et al.*[3] The lack of good agreement was attributed to experimental error. Hoffmann and Koopmann[8] designed an experiment to more accurately visualize the oscillations of small particles in an acoustic field and found modest agreement with the BFH model. More recently Gonzàlez, Hoffmann, and Gallego[6] (hereinafter GHG) conducted experiments on particles entrained into acoustic standing waves using laser particle illumination and digital image capturing methods. GHG defined the quantity,

$$\tau^* = \omega\tau = \frac{\omega \rho_p d_p^2}{18 \mu_f}, \quad (3)$$

as the relaxation number; an"acoustic" Stokes number. Here τ is the particle relaxation time and ω is the angular acoustic frequency. GHG conducted experiments for τ^* ranging from 0.06 to 10. Their results agree with the predictions of the BFH model.

For moderately strong acoustic waves and heavy particles in air the BFH model predictions of particle velocity amplitudes agree with the experimental data. However, several questions remain unanswered about the physics of small particle behavior in sound waves and the validity of the BFH model across a range of conditions. In the present study, we address the following questions:

(1) Over what ranges of relaxation number and fluid-to-particle density ratio does the BFH model remain accurate?

(2) What are the dominant forces in Eq. (1) that influence particle motion in an acoustic wave?

III. GOVERNING EQUATIONS

We recast Eq. (1) in a dimensionless form convenient for modeling particle motion in an acoustic wave. Let $u_i^* = u_i/U_0$ and $v_i^* = v_i/U_0$ be the dimensionless velocities of the fluid and particle, respectively, in the ith direction. Let t^* be the dimensionless time ωt and $x_i^* = (\omega/U_0)x_i$ be the dimensionless distance. The length scale (U_0/ω) is the displacement amplitude of a fluid element in the sound wave. Thus the dimensionless time is measured in units of the acoustic period, and the dimensionless particle position is measured relative to the travel distance of a fluid particle in the acoustic wave. The resulting dimensionless form of Eq. (1) is

$$\frac{dv_i^*}{dt^*} = \frac{(u_i^* - v_i^*)}{\tau^*} + \frac{3\,\epsilon}{\sqrt{2\tau^*}}\int_0^{t^*} \frac{\frac{d}{ds}(u_i^* - v_i^*)}{\sqrt{t^* - s}}ds + \epsilon^2\{\frac{Du_i^*}{Dt^*} + \frac{1}{2}(\frac{du_i^*}{dt^*} - \frac{dv_i^*}{dt^*})\} - (1-\epsilon^2)G, \quad (4)$$

where $\epsilon^2 = (\rho_f/\rho_p)$. To simplify the discussion in this section, we eliminate the index notation and consider particle motion in a single direction. Let $k = (\omega/c)$ be the acoustic wave-number, where c is the speed of sound. The traveling wave characteristic $(kx - \omega t)$ is written as $(Kx^* - t^*)$, where the Mach number $K = U_0/c \ll 1$. This characteristic prescribes a spatial variation of the fluid velocity that depends on the speed of sound and across which the particle moves.

We prescribe the acoustic fluid velocity as a single tone sinusoid, $u^* = \sin(Kx^* \pm t^*)$, where $x^* = \int v^* dt^*$, and v^* is the dimensionless velocity of the particle. It should be noted that $u^*du^*/dx^* = K\sin(Kx \pm t^*)\cos(Kx \pm t^*)$, and since $K \ll 1$, the displacement of a particle within an acoustic wave is negligible and Eq. (4) is nearly linear.

Equation (4) emphasizes the importance of three non-dimensional parameters in prescribing particle motion: τ^*, ϵ, and G. The parameter τ^* is the response time of the particle relative to the acoustic cycle time. The density ratio ϵ^2 affects the magnitude of the fluid inertial forces acting on the particle. $G \equiv g/U_o\omega$ is the ratio of the gravitational acceleration to that of a fluid particle in a sound wave. Note that Eq. (2) can be derived from Eq. (4) by setting K, ϵ and G equal to zero.

It should be noted that our undisturbed flow (far away from the particle) $u = \sin(kx - \omega t)$ satisfies the the Navier–Stokes equations (in one spatial dimension) under the two conditions of zero viscosity and zero vorticity. The derivation of $u = \sin(kx \pm \omega t)$ from the Navier–Stokes equations is described in many textbooks (e.g., Ref. 10). However, the disturbance flow around the particle is a Stokes flow which is viscous and rotational. Furthermore, the incompressibility condition, $\partial u_i/\partial x_i = 0$, is satisfied near a particle subjected to an acoustic wave under the conditions of our study:

$$\frac{d_p}{\lambda} \ll 1, \quad (5)$$

$$(\frac{d_p^2}{\nu})/(\frac{\lambda}{c}) \ll 1, \quad (6)$$

$$Re_p \ll 1, \quad (7)$$

where λ is the acoustic wavelength, d_p is the particle diameter, c is the speed of sound, and Re_p is the Reynolds number of particle motion. The velocity divergence $(\partial u_i/\partial x_i)$ is evaluated from the continuity equation as

$$\frac{\partial u_i}{\partial x_i} = -\frac{1}{\rho_f}(\frac{\partial \rho_f}{\partial t}) - \frac{u_i}{\rho_f}(\frac{\partial \rho_f}{\partial x_i}). \quad (8)$$

The term $(\frac{\partial \rho_f}{\partial t})$ on the RHS of Eq. (8) is negligible because the time scale of fluid density variation equals one quarter of the acoustic period, $(\lambda/4c)$, which is much larger than the viscous diffusion time scale, (d_p^2/ν), cf. Eq. (6), that controls the viscous stresses near the particle surface. Similarly, the term $(\frac{\partial \rho_f}{\partial x_i})$ in Eq. (8) is negligible because the length-scale of fluid density variation is $(\lambda/4)$, and thus the variation of ρ_f is negligible over distances equal to the particle diameter, cf. Eq. (5). Consequently, the acoustic flow interacting with a small particle can be considered locally incompressible under the conditions listed above.

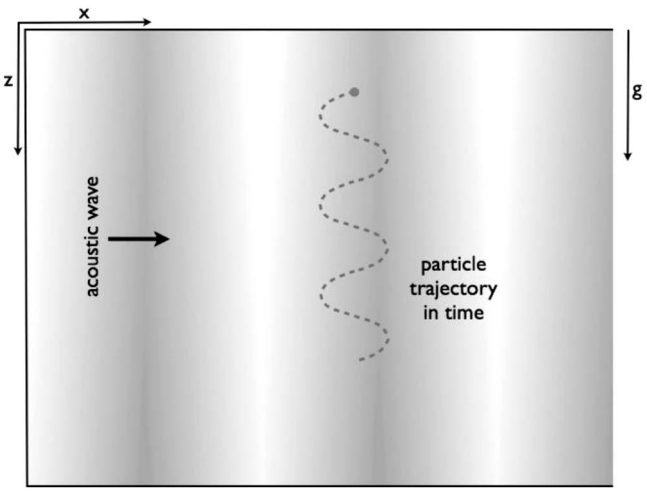

FIG. 1. Flow configuration.

It should be noted that Parmar *et al.*[18] have shown that under the above conditions (5)–(7) and Mach number $K = U_0/c \ll 1$, the compressibility effects on particle motion may be neglected.

IV. NUMERICAL SIMULATIONS

A. Flow configuration

The flow configuration is that of the experiment of GHG (Figure 1). A particle is allowed to move downward due to Earth's gravity. A horizontal, right traveling acoustic wave intersects the particle at $t^* = 0$.

B. Numerical method

The one dimensional fluid flow is prescribed analytically for a right traveling acoustic wave according to $u^* = \sin(Kx^* - t^*)$. No computational mesh is required. The particle velocity is obtained from the solution of Eq. (4) of particle motion.

We integrate Eq. (4) in time over the entire history of particle motion using the fourth-order Runge–Kutta method. For each time step, the Basset force is computed for previous time steps using trapezoidal integration of the stored values of $d(u^* - v^*)/dt^*$. A first order estimation of the Basset force is made at the current time step ($s = t^*$). The time increment Δt^* is prescribed such that $\tau^*/\Delta t^* > 4$.

We perform simulations for (ρ_p/ρ_f) ranging from 2 to 2500, corresponding to ϵ ranging from 0.02 to 0.7. For each value of ϵ, we compute the particle trajectories for 23 different values of the relaxation number τ^*, ranging from 0.06 to 10.5. We examine the linear, oscillatory particle motion by prescribing $K \leq 1 \times 10^{-3}$. In these simulations $0.005 < Re_p < 0.07$.

V. NUMERICAL RESULTS

A. Comparison with experimental results

Gonzàlez *et al.*[6] provide a series of integrated exposure photographs of particle trajectories. Figure 2 compares our computed (a) with the experimental (b) particle trajectory of Gonzàlez *et al.*[6] for $\tau^* = 0.06$, $\epsilon = 0.023$, and $K = 7 \times 10^{-6}$. The figure shows excellent agreement between the computed and measured trajectories. Figure 3 provides a similar comparison of the computed (a) and measured (b) trajectories for $\tau^* = 2.97$, $\epsilon = 0.023$, and $K = 3 \times 10^{-3}$.

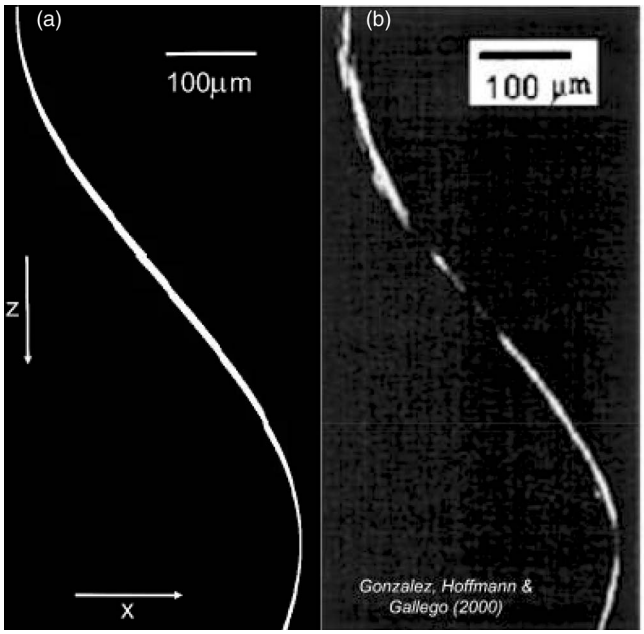

FIG. 2. Comparison between the computed (a) and measured (b) particle trajectory for $\tau^* = 0.06$ of Gonzàlez *et al.*[6]

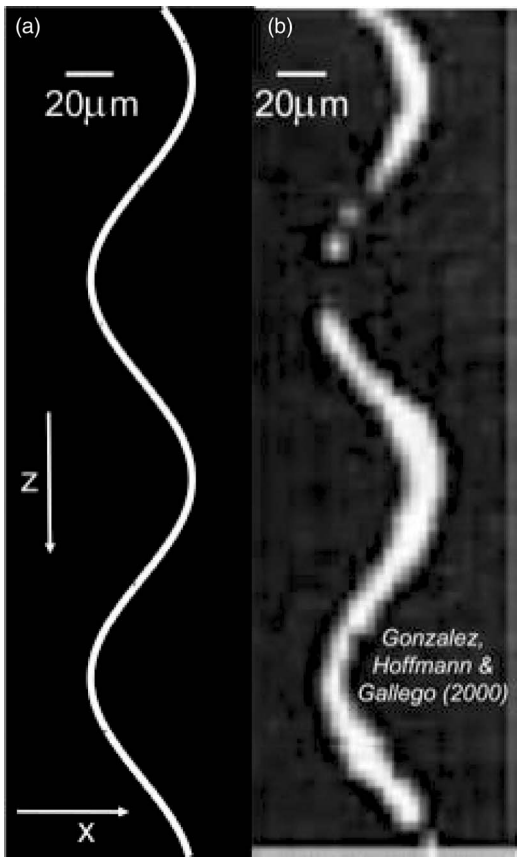

FIG. 3. Comparison between the computed (a) and measured (b) particle trajectory for $\tau^* = 2.97$ of Gonzàlez *et al.*[6]

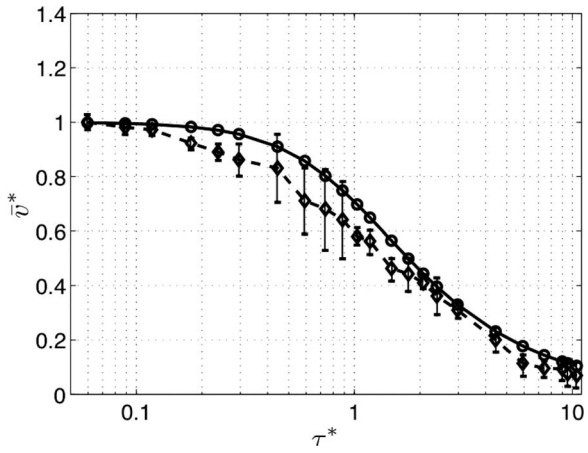

FIG. 4. Comparison of $\bar{v}^*$, between the present simulation (◯) and the experiments of GHG (◊) (τ^*-axis is log-scale). Upper and lower error bounds for the experimental data are shown by (-).

Figure 4 compares the computed and measured $\bar{v^*}$, the dimensionless particle velocity amplitude at the acoustic frequency, for values of τ^* used in the experiment of GHG, $\epsilon = 0.023$, and $7 \times 10^{-6} \leq K \leq 3 \times 10^{-3}$. Error bars are determined by GHG from the theoretical pixel resolution for each experiment. Our computed $\bar{v^*}$ agrees with the experimental data within the margins of pixel error for most τ^*. GHG[6] stated that the small amount of deviation observed between their experimental data and the BFH model for $\tau^* > 0.2$ is due to acoustic driver distortion at the frequencies used through this regime.

B. Effects of the density ratio

We examine the effect of the density ratio ϵ, defined as $\sqrt{\rho_f/\rho_p}$, on the particle motion. Our results show that after a transient period, the particle motion remains periodic at the acoustic frequency as ϵ increases. Thus we can describe the particle motion in terms of a velocity amplitude ($\bar{v^*}$) and phase ($\Delta\phi$) relative to the fluid velocity u^*. Figure 5 shows the variation of $\bar{v^*}$ and $\Delta\phi$ with τ^* for different values of ϵ. The particle velocity amplitude and phase for $\epsilon = 0$ (the BFH model) are shown in Figures 5(a) and 5(b), respectively, for comparison.

Figure 5(a) shows, as expected, that $\bar{v^*}$ decreases with τ^* for all values of ϵ simulated, and that the decay rate of $\bar{v^*}$ diminishes as ϵ increases. For $\tau^* < 0.2$, $\bar{v^*}$ is nearly independent of ϵ, and for $\epsilon \leq 0.2$, this independence persists to $\tau^* \approx 1$. As $\tau^* \to 10$, $\bar{v^*}$ increases with ϵ. This increase is relatively small for $\epsilon \leq 0.2$, but increases rapidly thereafter.

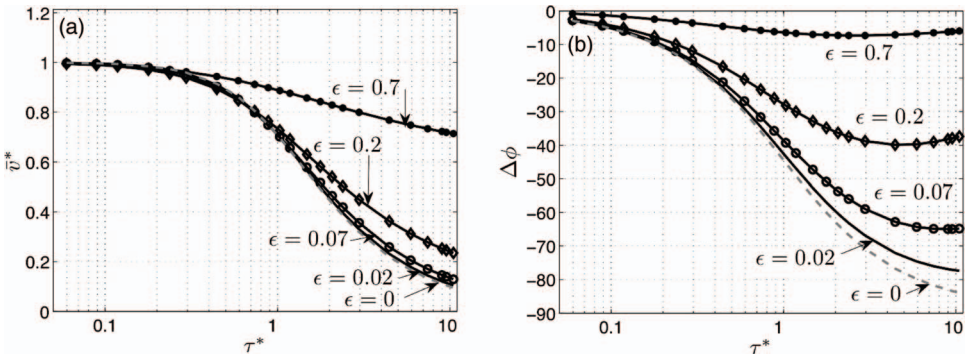

FIG. 5. (a) Particle velocity amplitude ($\bar{v^*}$) versus τ^* (τ^*-axis is log-scale). (b) Phase ($\Delta\phi$) between v^* and u^* versus τ^* (τ^*-axis is log-scale). Results are for ϵ equal to 0.02 (−), 0.07 (◯), 0.2 (◊), and 0.0 (−−).

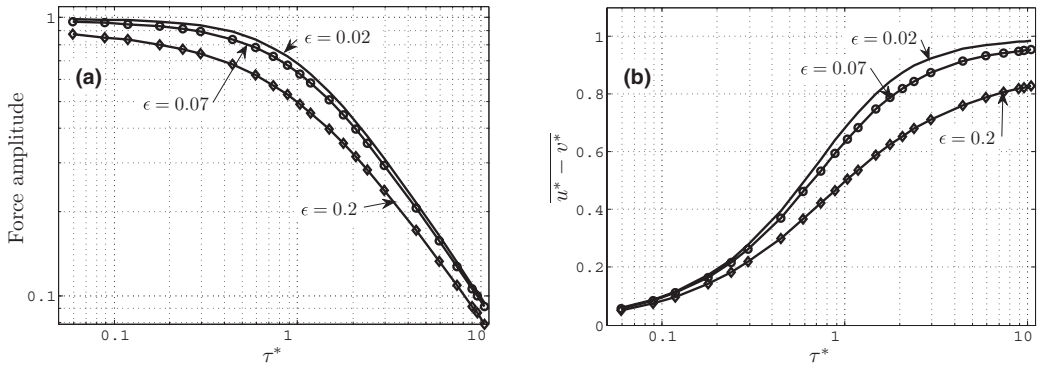

FIG. 6. (a) The Stokes force amplitude versus τ^* for ϵ equal to 0.02 (−), 0.07 (◯), and 0.2 (◊). Both axes are log-scales. (b) Effect of increasing τ^* on the relative velocity amplitude, $u^* - v^*$, for ϵ equal to 0.02 (−), 0.07 (◯), and 0.2 (◊). τ^*-axis is log-scale.

Figure 5(b) shows a similar trend, though the variation of the phase $\Delta\phi$ with ϵ is more pronounced. For a given $\bar{v^*}$, the oscillatory phase determines the instantaneous velocity and position of the particle. Thus the instantaneous particle velocity and position are more affected by increasing ϵ than is the velocity amplitude, $\bar{v^*}$.

Figure 5(a) shows that the BFH model, which assumes $\epsilon = 0$, is applicable for $\epsilon \leq 0.2$. It is accurate for predicting $\bar{v^*}$ up to $\tau^* \approx 1$. At $\tau^* = 10$, the BFH model underestimates $\bar{v^*}$ by 10%, 18% and 48% for $\epsilon = 0.02$, $\epsilon = 0.07$, and $\epsilon = 0.2$, respectively. Predicting the instantaneous position of the particle accurately is a more difficult test for the BFH model. The phase $\Delta\phi$ deviates in excess of 5° from the BFH model at $\tau^* \approx 5$ for $\epsilon = 0.02$, $\tau^* \approx 1$ for $\epsilon = 0.07$ and at $\tau^* \approx 0.5$ for $\epsilon = 0.2$.

In order to explain the results of Figure 5, we examine the behavior of the non-dimensional forces in Eq. (4). Our detailed analysis of these forces showed that, after a transient period, each force is oscillatory at the acoustic frequency for the values of K considered. Thus we represent each force with a magnitude and phase ($\Delta\phi$) relative to u^*. Hereinafter we refer to the non-dimensional forces by their dimensional names.

Equation (4) indicates that as $\epsilon \to 0$, i.e., for particles with large density, only the Stokes force contributes to particle motion in the direction of sound wave travel. For finite values of ϵ, the Stokes force depends implicitly on ϵ through particle velocity. Figure 6 shows the variation of Stokes force amplitude with τ^* for the range of $\epsilon = 0.02$ to $\epsilon = 0.2$. For this range, v^* is a weak function of ϵ (Figure 5(a)) and the Stokes force dominates particle motion.

Figure 6(a) shows that for $\epsilon \leq 0.2$, the Stokes force amplitude = 1 for small τ^* and decreases monotonically as $\tau^* \to 10$. The Stokes force is directly proportional to the relative velocity, $(u^* - v^*)$, and inversely proportional to τ^*. The relaxation number τ^* is the ratio of the particle's relaxation time to the acoustic period (see Eq. (3)). It measures the particle's response time to acoustic changes in flow direction. A particle's response time decreases with increasing fluid viscosity, and decreasing particle mass and acoustic frequency. As $\tau^* \to 0$, the particle responds instantly to the fluid motion and $(u^* - v^*) \to 0$. The Stokes force, $(u^* - v^*)/\tau^*$, approaches a value of one in this limit. With increasing τ^*, the particle cannot accelerate with the changing fluid velocity, and v^* decreases as shown in Figure 5, thus $(u^* - v^*)$ increases. However, $(u^* - v^*)$ increases more slowly than τ^* and the Stokes force decreases monotonically as $\tau^* \to \infty$. This montonic reduction can be explained as follows. As the particle relaxation number τ^* increases, the particle velocity oscillation, v^*, decreases. Thus, as $\tau^* \to \infty$, $v^* \to 0$, and the velocity difference $(u^* - v^*) \to u^*$. However, the prescribed fluid velocity of the acoustic wave, $u^* = \sin(Kx^* - t^*)$, has a maximum amplitude = 1. Therefore, as $\tau^* \to \infty$, $(u^* - v^*) \to 1$, resulting in $(u^* - v^*)/\tau^* \to 0$. Figure 6(b) shows the effect of increasing τ^* on the relative velocity $(u^* - v^*)$ for three different ϵ values. It is clear that $(u^* - v^*)$ approaches its maximum value of 1 asymptotically as τ^* increases, and the smaller the value of ϵ (i.e., heavier particle) the sooner the peak is reached. Figure 7(a) shows the variation with τ^* of the amplitudes of the Stokes, Basset, pressure gradient, and virtual mass forces

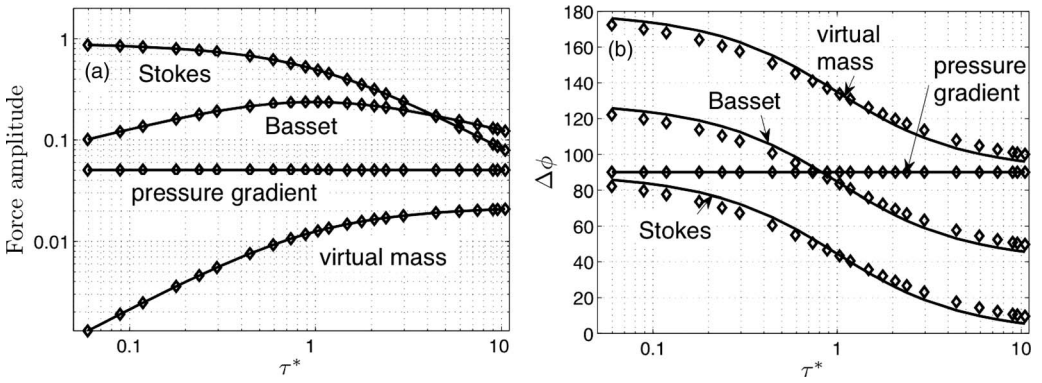

FIG. 7. (a) Non-dimensional amplitudes of the Stokes, Basset, pressure gradient, and virtual mass forces versus τ^* for $\epsilon = 0.2$ (both axes are log-scale). (b) Phase of forces relative to that of u^* (τ^*-axis is log-scale). Phase results are for ϵ equal to 0.02 (−) and 0.2 (◊).

for $\epsilon = 0.2$. The Stokes force is the largest of these forces for $\tau^* < 4$. The Basset force reaches parity with the Stokes force at $\tau^* \approx 4$. Following the Stokes and Basset forces, the pressure gradient force is the third most significant. The virtual mass force has the least impact on a particle.

In Figure 6(a) the curves describing the variation of Stokes force amplitude with τ^* are similar for the three values of ϵ plotted. We also examined the Basset, pressure gradient, and virtual mass forces for all values of ϵ simulated. Though the magnitudes of non-Stokes forces change with ϵ the shape of each curve for $\epsilon < 0.2$ remains similar to that for $\epsilon = 0.2$. The shapes of these curves and their significance as a function of ϵ are described below.

Figure 7(a) shows that the Basset force is considerably smaller than the Stokes drag but the difference between them diminishes as $\tau^* \to 10$. The observed maximum of the Basset force at $\tau^* \approx 1$ is due to the competition between $d(u^* - v^*)/dt^*$, which is established by the Stokes force, and the slowly varying divisor $\sqrt{\tau^*}$. In Figure 7(a), the Basset force amplitude is greater than 0.1 of the Stokes force amplitude for all values of τ^* and $\epsilon = 0.2$. We examined the Basset force amplitude for all considered values of ϵ and found that it is larger than 0.1 of the Stokes force amplitude for $\tau^* \geq 5$ and $\epsilon = 0.02$, and $\tau^* \geq 0.5$ for $\epsilon = 0.07$. However, these results are not plotted due to space limitations. Figure 7(b) shows that the Basset force maintains a phase lead over the Stokes force of 40° and thus augments the Stokes force. Equation (4) shows that the pressure gradient and virtual mass forces are proportional to ϵ^2, of which the former has more impact on the particle motion, as shown in Figure 7(a), for the conditions described. The pressure gradient force is proportional to the time rate of change of fluid inertia and thus its effect increases as the density of the fluid increases relative to that of the particle. Figure 7(a) shows that the amplitude of the pressure gradient force does not vary with τ^* since this force depends only on fluid velocity u^*. Similarly, Figure 7(b) shows that the phase of the pressure gradient force is independent of τ^*. This phase approaches that of the Stokes force as $\tau^* \to 0$, and thus the former augments the latter in this case. At $\tau^* \approx 0.8$, the pressure gradient force augments the Basset force, and as $\tau^* \to 10$ the pressure gradient force is in phase with the virtual mass force.

The virtual mass force is caused by the particle as it accelerates and displaces its surrounding fluid. This force increases as the density of the fluid increases relative to that of the particle as shown in Eq. (4). The virtual mass force approaches zero as $\tau^* \to 0$, since $v^* \to u^*$, resulting in $d(u^* - v^*)/dt^* \to 0$ at this limit, as shown in Figure 7(a). For small ϵ, Figure 5(a) shows that the particle velocity amplitude asymptotically approaches zero as $\tau^* \to 10$ and thus $d(u^* - v^*)/dt^* \to du^*/dt^*$. Since $u^* = \sin(Kx^* \pm t^*)$, then $du^*/dt^* = \pm\cos(Kx^* \pm t^*)$ and the relative fluid acceleration at the particle position has an amplitude = 1. Under these conditions, an examination of Eq. (4) shows that the virtual mass force approaches an amplitude of $\epsilon^2/2$. Figure 7(a) confirms that the virtual mass, for $\epsilon = 0.2$, approaches an asymptotic value of $\epsilon^2/2 = 0.02$ at $\tau^* = 10$.

For $\epsilon = 0.2$, the combined amplitude of the pressure gradient and virtual mass forces is more than 0.1 of the Stokes force for $\tau^* \geq 0.7$. We examined the pressure gradient and virtual mass force

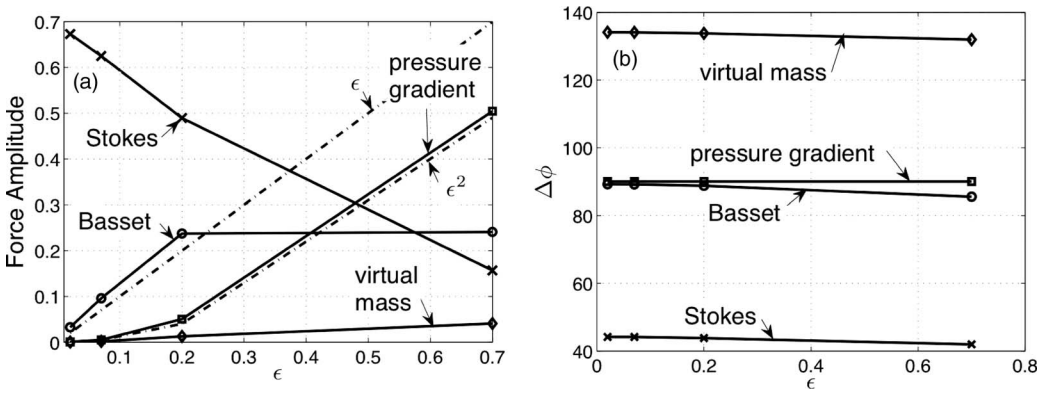

FIG. 8. Amplitudes **(a)** and phases, $\Delta\phi$, **(b)** versus ϵ at $\tau^* = 1.0$ for the Stokes, Basset, pressure gradient, and virtual mass forces.

amplitudes for all values of ϵ simulated. The combined pressure gradient and virtual mass force amplitudes are smaller than 0.1 of the Stokes drag amplitude for $\epsilon \leq 0.07$. These results are not plotted due to space limitations.

We also performed an analysis of all forces on the particle for $\epsilon = 0.7$. Again, these results are not shown due to space limitations. For $\epsilon = 0.7$, the pressure gradient and virtual mass forces, which are proportional to ϵ^2, significantly affect the relative velocity, $(u^* - v^*)$, and in turn the Stokes and Basset forces. For $\epsilon = 0.7$, the Stokes drag is not the dominant force and its dependence on τ^* is not similar to the trend shown in in Figure 6(a). Equation (4) shows that the pressure gradient and virtual mass terms are not explicit functions of τ^*. They tend to reduce the dependence of the Stokes and Basset forces on τ^*. Consequently, the dependence of $\bar{v^*}$ and its phase, $\Delta\phi$, upon τ^* is reduced for $\epsilon = 0.7$ in Figure 5. In order to show the direct dependence of the different forces affecting the particle motion on ϵ, Fig. 8 displays the variation of the amplitude and phase of these forces with ϵ for $\tau^* = 1.0$. The figure shows that:

(i) The pressure gradient force increases monotonically with ϵ. As the pressure gradient force becomes dominant, it generates most of the particle acceleration. Equation (4) shows that the pressure gradient force is a function of (u^*) and *not* $(u^* - v^*)$ like the Stokes, Basset, and added mass forces. Thus, the pressure gradient force reduces $(u^* - v^*)$. Consequently, the Stokes force, being proportional to $(u^* - v^*)$, decreases with increasing ϵ.

(ii) The Basset force is proportional to both ϵ and $d(u^* - v^*)/dt^*$. It increases up to $\epsilon = 0.2$, then it remains invariant with the further increase of ϵ because the pressure gradient force reduces $(u^* - v^*)$ considerably for large ϵ.

(iii) The added (virtual) mass force depends on both ϵ^2 and $(u^* - v^*)$. Consequently, the virtual mass force increases with ϵ at a much smaller rate than that of ϵ^2. The phase of each force component decreases only slightly with ϵ.

C. Discussion

We note that our use of Eq. (4) which was derived for particle motion in an incompressible flow is justified given that the magnitude of the divergence of the fluid velocity, $\vec{\nabla}^* \cdot \vec{u}^*$, is proportional to the Mach number K which is $\ll 1$ in our simulations. Particle motion in incompressible periodic flows have been considered by many authors, including Chang and Maxey,[4] Mie *et al.*,[16] Mei and Adrian,[15] Mei,[14] and Kim *et al.*[9] The acoustic flow considered in our study is in principle different from the flows in the previous studies due to the wave characteristic, $(Kx^* - t^*)$, which prescribes a spatial variation in the flow that depends on the speed of sound. The Lagrangian motion of the particle is affected by this spatially inhomogeneous flow field. However, we find that the effects of

this inhomogeneity are very small for $K \leq 1 \times 10^{-3}$. In most fluids, this range of K extends to moderate acoustic amplitudes.

In this study, we did not consider nonlinear sound waves or the effects of compressibility on fluid properties. For high amplitude sound waves, fluid streaming[11,19] and fluid harmonic distortion[10] are also present and these in turn affect particle velocity. Furthermore, Mednikov[13] suggests that the inter-cycle variation of viscosity and density generates particle drift and harmonic distortion. We ignore these effects since they are either of order K or K^2.

VI. CONCLUSIONS

We have performed a large number of numerical simulations using Eq. (4) to study the motion of a small particle in a linear acoustic wave. The particle relaxation number, τ^*, ranged from 0.06 to 10, particle to fluid density ratios ranged from 2500 ($\epsilon = 0.02$) to 2 ($\epsilon = 0.7$) and acoustic velocities ranged from $7 \times 10^{-6} \leq K \leq 1 \times 10^{-3}$. The main conclusions are as follows:

(1) The results of our numerical simulations using Eq. (4) agree with the recent experimental data of Gonzàlez *et al.*[6] for heavy particles oscillating in an airborne ($\rho_p/\rho_f = 2500$) acoustic wave over a range of τ^* spanning two orders of magnitude.
(2) The model of Brandt *et al.*[3] is applicable for $\epsilon \leq 0.2$. It predicts the particle velocity amplitude accurately up to relaxation number $\tau^* \approx 1$.
(3) The Stokes force is the most dominant in controlling particle motion for $\epsilon = \sqrt{\rho_f/\rho_p} < 0.2$. Within this regime, it is appropriate to consider the Basset, pressure gradient, and virtual mass forces as "higher order" corrections to the Stokes force.
(4) The magnitude of the Basset force surpasses that of the Stokes force for $\epsilon = 0.2$ and $\tau^* \geq 4$.
(5) All forces in Eq. (4) should be computed when simulating particle motion in an acoustic wave for $\epsilon > 0.2$.

ACKNOWLEDGMENTS

The simulations presented in this paper were performed on a SGI Altix ICE 8200 cluster. The authors wish to acknowledge the Army Research Laboratories—DoD Supercomputing Resource Center (ARL-DSRC) for providing this resource.

[1] A. B. Basset, *A Treatise on Hydrodynamics*, Vol. 2 (George Bell and Sons, London, 1888).
[2] J. Boussinesq, "Sur la résistance qu'oppose un liquide indéfini en repos, sans pesanteur, au mouvement varié d'une sphère solide qu'il mouille sur toute sa surface . . . ," C.R. Acad. Sci. Paris **100**, 935–937 (1885).
[3] O. Brandt, H. Freund, and E. Hiedemann, "Zur theorie der akustischen koagulation," Kolloid-Z **77**, 103–115 (1936).
[4] E. J. Chang and M. R. Maxey, "Unsteady flow about a sphere at low to moderate Reynolds number. Part 1. Oscillatory motion," J. Fluid Mech. **303**, 133–153 (1994).
[5] H. Faxén, "Der Widerstand gegen die Bewegung einer starren Kugel in einer zähen flüssigkeit, die zwischen zwei parallelen ebenen Wänden eingeschlossen ist," Annalen der Physik **373**(10), 89–119 (1922).
[6] I. Gonzàlez, T. L. Hoffmann, and J. A. Gallego, "Precise measurements of particle entrainment in a standing-wave acoustic field between 20 and 3500 Hz," J. Aerosol Sci. **31**, 1461–1468 (2000).
[7] F. T. Gucker and G. J. Doyle, "The amplitude of vibration of aerosol droplets in a sonic field," J. Phys. Chem. **60**, 989–996 (1956).
[8] T. L. Hoffmann and G. H. Koopmann, "A new technique for visualization of acoustic particle agglomeration," Rev. Sci. Instrum. **65**, 1527–1536 (1994).
[9] I. Kim, S. Elghobashi, and W. A. Sirignano, "On the equation for spherical particle motion: effect of Reynolds and acceleration numbers," J. Fluid Mech. **367**, 221–253 (1998).
[10] L. E. Kinsler, A. R. Frey, A. B. Coppens, and J. V. Sanders, *Fundamentals of Acoustics*, 4th ed. (Wiley, 2000).
[11] M. J. Lighthill, "Acoustic streaming," J. Sound Vib. **61**, 391–418 (1978).
[12] M. R. Maxey and J. J. Riley, "Equation of motion for a small rigid sphere in a nonuniform flow," Phys. Fluids **26**, 883–889 (1983).
[13] E. P. Mednikov, *Acoustic Coagulation and Precipitation of Aerosols* (Consultants Bureau Enterprises, Inc., 1965).
[14] R. Mei, "Flow due to an oscillating sphere and an expression for unsteady drag on the sphere at finite Reynolds number," J. Fluid Mech. **270**, 133–174 (1994).
[15] R. Mei and R. J. Adrian, "Flow past a sphere with a oscillation in the free-stream velocity and unsteady drag at finite Reynolds number," J. Fluid Mech. **237**, 323–341 (1992).

[16] R. Mei, C. J. Lawrence, and R. J. Adrian, "Unsteady drag on a sphere at finite Reynolds number with small fluctuations in the free stream-velocity," J. Fluid Mech. **233**, 613–631 (1991).
[17] C. W. Oseen, *Hydrodynamik* (Akademische Verlagsgesellschaft, Leipzig, 1927; Dover, 1945), Vol. 2.
[18] M. Parmar, A. Haselbacher, and S. Balachandar, "Generalized Basset–Boussinesq–Oseen equation for unsteady forces on a sphere in a compressible flow," Phys. Rev. Lett. **106**, 084501 (2011).
[19] N. Riley, "Steady streaming," Annu. Rev. Fluid Mech. **33**, 43–65 (2001).